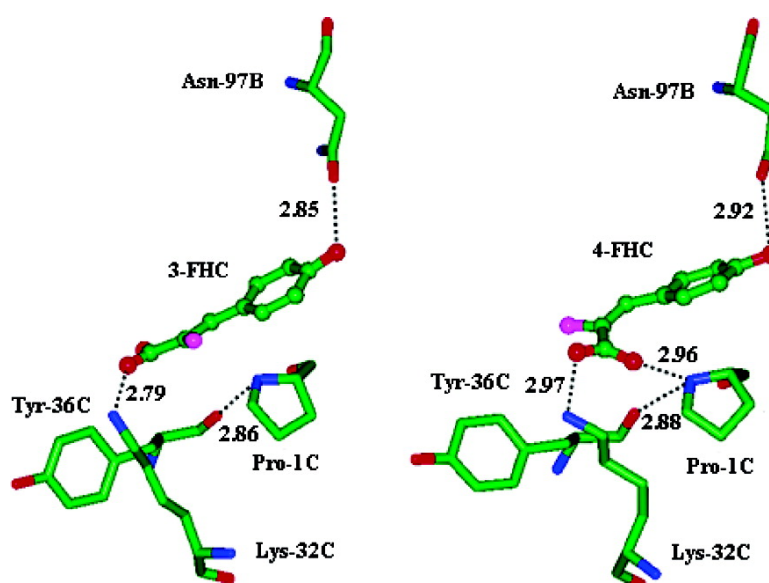


Some Insights into the Stereochemistry of Inhibition of Macrophage Migration Inhibitory Factor with 2-Fluoro-*p*-hydroxycinnamate and Its Analogues from Molecular Dynamics Simulations

Shulin Zhuang, Jianwei Zou, Yongjun Jiang, Xiang Mao, Bing Zhang, Haichun Liu, and Qingsen Yu

J. Med. Chem., 2005, 48 (23), 7208-7214 • DOI: 10.1021/jm050562z • Publication Date (Web): 13 October 2005

Downloaded from <http://pubs.acs.org> on March 29, 2009



More About This Article

Additional resources and features associated with this article are available within the HTML version:

- Supporting Information
- Links to the 1 articles that cite this article, as of the time of this article download
- Access to high resolution figures
- Links to articles and content related to this article
- Copyright permission to reproduce figures and/or text from this article

[View the Full Text HTML](#)

Some Insights into the Stereochemistry of Inhibition of Macrophage Migration Inhibitory Factor with 2-Fluoro-*p*-hydroxycinnamate and Its Analogues from Molecular Dynamics Simulations

Shulin Zhuang,^{†,‡} Jianwei Zou,^{*,‡} Yongjun Jiang,[‡] Xiang Mao,[§] Bing Zhang,^{†,‡} Haichun Liu,^{†,‡} and Qingsen Yu^{†,‡}

Department of Chemistry, Zhejiang University, Hangzhou 310027, P. R. China, Ningbo Institute of Technology, Zhejiang University, Ningbo 315104, P. R. China, and Department of Biochemistry and Molecular Biology, M. D. Anderson Cancer Center, The University of Texas, Box 117, 1515 Holcombe Boulevard, Houston, Texas 77030

Received June 15, 2005

Macrophage migration inhibitory factor (MIF) exhibits tautomerase activity on phenylpyruvate and has *E*-stereochemistry preference. To investigate the binding modes of its competitive inhibitors and evaluate their binding affinities, molecular dynamics simulations together with MM-PBSA (molecular mechanics Poisson–Boltzmann surface area) analysis were performed on MIF complexed with (*E*)-2-fluoro-*p*-hydroxycinnamate and five analogues. Pro-1 was discovered to form a bifurcated hydrogen bond between its protonated nitrogen and carboxylate oxygens of *E*-ligands and Tyr-36. No hydrogen bonds were found between Pro-1 and *Z*-ligands. This distinct binding characteristic of *E*- and *Z*-ligands with Pro-1 may be the main factor for the large difference in their binding affinities, which is consistent with the previous report that Pro-1 is essential for the catalytic activity of MIF. MM-PBSA analysis revealed that energy components including van der Waals, electrostatic, and hydrophobic interactions are in favor of binding, among which electrostatic interactions are predominant to the binding affinity difference.

Introduction

Macrophage migration inhibitory factor (MIF), originally identified as a T-cell-derived cytokine, is an integral component of the host antimicrobial alarm system and stress response that promotes the proinflammatory functions of immune cells.¹ Interestingly, it also shows many characteristic properties different from those of proinflammatory cytokines, including both structural and functional aspects, and encompasses MIF expression, localization, secretion, and target cell interaction.²

MIF exists as a homotrimer with each monomer containing two antiparallel α -helices packed against a four-strand β -sheet ($\beta/\alpha/\beta$) (Figure 1). Its structure is unique, and no significant sequence homologies have been found between MIF and any other known proteins.^{3,4}

MIF has been shown to be involved in a variety of diseases, including sepsis, acute respiratory distress syndrome (ARDS), asthma, atopic dermatitis, rheumatoid arthritis (RA), nephropathy, and tumors.^{5,6} Experimental data show that MIF could act as a phenylpyruvate tautomerase (PPT).⁷ Potent tautomerase inhibitors may be useful in the treatment of MIF-related diseases. Since the detailed understanding of the biological functions of MIF has not yet been established, enzymology studies could serve as primary methods to elucidate the molecular basis of MIF biological functions.

A series of cinnamate analogues have been designed recently as the competitive inhibitors of MIF⁸ as phe-

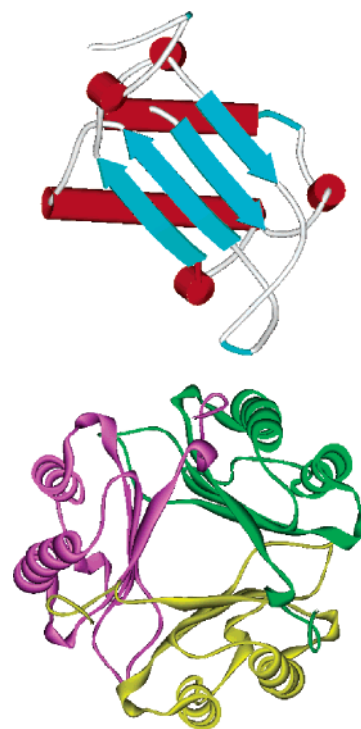


Figure 1. Top: monomer of MIF. α -Helices and β -sheets were colored red and cyan, respectively. Bottom: structure of homotrimer of MIF. Three monomers were in different color.

nylpyruvate tautomerase. The data reveal an interesting *E*-stereochemistry preference in that all the *E*-ligands are better inhibitors of MIF than the corresponding *Z*-ligands, which indicates that the *E*-ligands have a more tight binding ability with MIF than the *Z*-ligands, although *Z*-ligands are thermodynamically

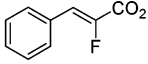
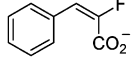
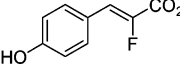
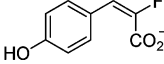
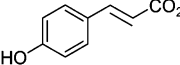
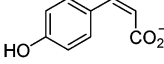
* To whom correspondence should be addressed. Phone: 086-5574-88229516. Fax: 086-574-88229516. E-mail: jwzou@nit.net.cn.

[†] Department of Chemistry, Zhejiang University.

[‡] Ningbo Institute of Technology, Zhejiang University.

[§] The University of Texas.

Table 1. Inhibition Data of Cinnamate Stereoisomers⁸

Name	Configuration	Cinnamate Stereoisomers	Ki
1-FHC	Z		2.33mM
2-FHC	E		73μM
3-FHC	Z		0.48mM
4-FHC	E		1.7μM
5-FHC	Z		0.21mM
6-FHC	E		1.5μM

more stable. Experimental studies have indicated *E*-stereochemistry preference of MIF, but there is no report on the elucidation of this phenomenon at the atomic level.

Stereochemistry is an important factor that should be considered when studying stereoisomer–receptor interaction. Different stereoisomers can have a remarkable effect on the biological activity, and changes in stereochemistry might cause considerable loss of binding potency.^{9–13} Molecular dynamics simulation could serve as a powerful tool for understanding mechanisms of the stereochemistry of recognitions, interactions, and dynamics of the stereoisomer–receptor complex.

The molecular mechanics Poisson–Boltzmann surface area (MM-PBSA) method is a versatile tool for calculating the binding free energy of macromolecular systems, which incorporates the effects of thermal averaging via postprocessing of an ensemble of protein–ligand configurations with a force field/continuum model potential.^{14,15} This approach has been successfully applied to the calculation of the binding free energy for ligand–protein interactions,^{15–18} DNA–drug interaction,¹⁹ and RNA–protein interactions.^{20,21}

To investigate the interaction properties with MIF and ligands, molecular dynamics (MD) simulations have been performed for the systematic structural studies of *E*- and *Z*-ligands complexed with MIF. MM-PBSA analysis based on MD trajectories was used to decompose the contributions of different energy components on ligand binding.

The information obtained from this study could help to clarify enzymatic mechanism for MIF and shed light on the relationship between its biological functions and enzymatic activity. It could also provide a structure-based guide on the design of inhibitors/potential drugs in the treatment of a variety of inflammatory and immune-related diseases associated with MIF.

Computational Details

System Setups. The crystal structure of (*E*)-2-fluoro-*p*-hydroxycinnamate (4-FHC in Table 1) with macrophage migration inhibitory factor (PDB accession code 1MFI²²) was used as the starting structure in the

present MD simulation. The complex structure of MIF with other five analogues (1-FHC, 2-FHC, 3-FHC, 5-FHC, 6-FHC) were built using 1MFI as the template in the DS modeling program.²³ Using structurally similar compounds could facilitate the construction of each protein/ligand complex and help ensure that the ligands are placed in a reasonable starting conformation.²⁴

The ligand located in the active site of the C chain was kept, and the other two ligands in the complex were removed. Crystallographic water molecules were discarded because no crystallographic waters are present in the active site. The N-terminal proline residue was considered as the protonated state, according to the experimental p*K*_a data available.²⁵ For other ionizable residues, default protonation states in the AMBER 7 package²⁶ were employed. One Na⁺ is added to maintain the electroneutrality of the systems. All solutes were surrounded by a truncated octahedron periodic box of water molecules described by the TIP3P potential²⁷ extended to a distance of 10 Å from solute atoms. The numbers of TIP3P water molecules in the six simulation systems are all around 6100.

Quantum Mechanics Calculations. Owing to the lack of parameters needed for the ligands in the Cornell et al. force field,²⁸ the missing parameters were developed. Optimization of the six ligands listed in Table 1 was first carried out at the HF/6-31G* level with the Gaussian 98 package.²⁹ Electrostatic potentials (ESP) were then obtained using Merz–Singh–Kollman van der Waals parameters.³⁰ Fitting charges to the ESP was performed with the RESP program³¹ implemented in the AMBER 7 package. GAFF²⁶ force field parameters and RESP partial charges were assigned using the ANTECHAMBER module in the AMBER 7 package.

To explore the intrinsic relative stability of the *Z*- and *E*-isomer, all six ligands were reoptimized at the B3LYP/6-311++G(d,p) level of theory.^{32–34} The solvent (water) effect on the relative stability of these ligands was also examined with the polarized continuum model (PCM).³⁵

Molecular Dynamics Simulations. All simulations were carried out using the AMBER 7 package with the Cornell et al. all-atom force field and parameters developed in this work. Long-range electrostatic interactions were treated with the particle mesh Ewald (PME) procedure³⁶ using a cubic B-spline interpolation and a 10^{−5} tolerance set for the direct-space and with a value of 12 Å for the nonbonded cutoff. Bond lengths involving hydrogen atoms were constrained using the SHAKE algorithm.³⁷ Minimization was performed with the SANDER module at constant volume, and 2500 cycles of steepest descent minimization followed by 2500 cycles of conjugated gradient method were applied until the root-mean-square of the Cartesian elements of the gradient between two consecutive structures was smaller than 0.0001 kcal mol^{−1} Å^{−1}. The time step for all MD simulations was 2 fs, and translational center-of-mass motions were removed every 1000 steps. After energy minimization, the solvated system was heated from 0 to 300 K at constant volume over the initial 50 ps. Subsequent isothermal isobaric ensemble (NPT) MD was used for 1 ns; this time scale is validated by NMR studies that show that the backbone of MIF exists in a

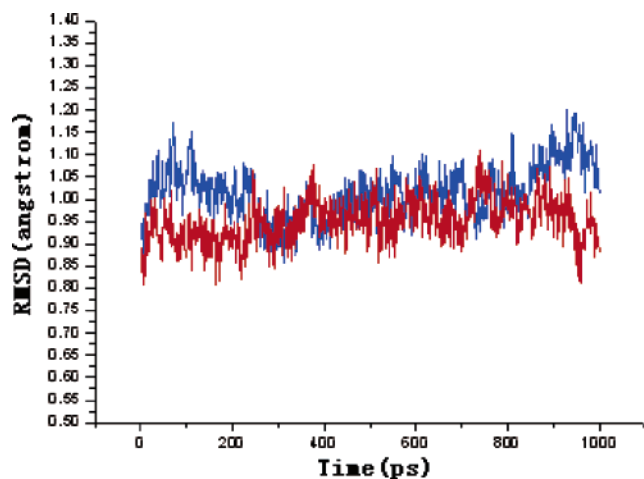


Figure 2. C α rmsd compared to the initial minimized complex structures as a function of time: (blue) MIF/3-FHC complex; (red) MIF/4-FHC complex. The averaged C α rmsd values for the MIF/3-FHC and MIF/4-FHC complexes are 1.01 and 0.95 Å, respectively.

rigid structure on the nanosecond to picosecond time scale.³⁸ Trajectories were analyzed using the PTRAJ modules.

Thermodynamic Calculations. Binding free energy analysis was carried out with the MM-PBSA approach³⁹ supplied with AMBER 7 package.

The snapshots of the solute were sampled from the last 400 ps single trajectory with an intervals of 8 ps. The molecular mechanical energies in the gas phase (ΔE_{gas}) were calculated using the SANDER module. Estimation of the polar solvation free energy (ΔG_{pb}) was performed with a finite-difference Poisson–Boltzmann electrostatic continuum method using the program Delphi II.⁴⁰ The nonpolar solvation free energy ($\Delta G_{\text{nonpolar}}$) was described by

$$\Delta G_{\text{nonpolar}} = \lambda \text{SASA} + b$$

where SASA is the solvent accessible surface area⁴¹ calculated with the MOLSURF program⁴² and λ and b are 0.005 42 kcal mol⁻¹ Å⁻² and 0.92 kcal mol⁻¹, respectively. The dielectric boundary was taken as the solvent accessible surface defined by a 1.4 Å probe sphere and by spheres centered on each atom with radii taken from the PARSE parameter set (H = 1.0, C = 1.7, N = 1.5, O = 1.4),⁴³ with a value of 1.47 for fluorine. The partial charges of the solute atoms were taken from the Cornell et al. force field to be consistent with the energetics of the explicit simulations.⁴⁴ The dielectric constant inside and outside the solute was set to 1 and 80, respectively. For the Poisson–Boltzmann calculation, a cubic lattice with linear dimensions ~80% larger than the longest dimension was applied with a 0.4 Å grid spacing and potentials at the boundaries of the finite-difference lattice were set to the sum of Debye–Huckel potentials.¹⁹ To coincide with experimental conditions used for determining the binding affinity, the effect of salt was taken into account with an ionic strength of 0.1 M.

Results and Discussion

The 1 ns NPT MD simulations were successfully performed separately on complexes of MIF with six

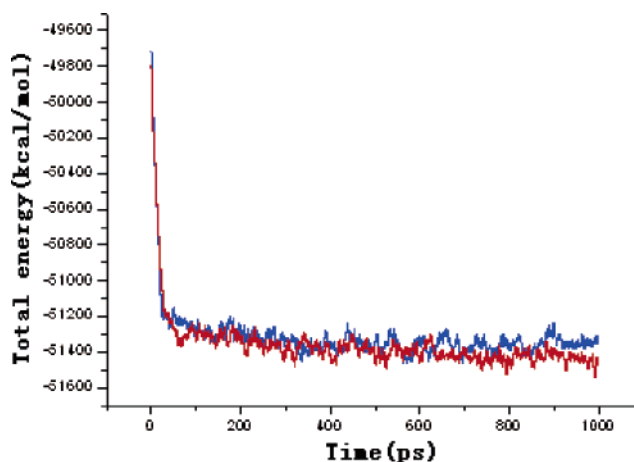


Figure 3. Total energy (kcal/mol) as a function of time: (blue) MIF/3-FHC complex; (red) MIF/4-FHC complex.

Table 2. Hydrogen Bond upon Complex Formation^a

ligands	atom	residues ^b	% occupied ^c
1-FHC			
2-FHC	O2	Pro-1C	76.23
3-FHC	H4	Asn-97B	99
4-FHC	H4	Asn-97B	93.6
	O2	Pro-1C	82.3
5-FHC	H5	Asn-97B	97.5
6-FHC	H4	Asn-97B	96.9
	O2	Pro-1C	88.9

^a The hydrogen bond defined by distances between heavy atoms of donor and acceptor of no more than 3.5 Å and the angles of donor and acceptor diatomic groups of no less than 120°. ^b Symbols of residues are explained in the text. ^c % occupied, to evaluate the stability and the strength of the hydrogen bonds.

ligands. The root-mean-squared deviation (rmsd) fluctuations of backbone atoms compared to those of the initial minimized complex structures were obtained over a 1 ns NPT trajectory. Figure 2 shows the rmsd of the main chains of the MIF/3-FHC and MIF/4-FHC complexes, and Figure 3 is the plot of the total energies of these two systems as a function of time. These two figures together indicate that the solvated system had reached equilibrium after 300 ps of the NPT MD simulation. The averaged C α rmsd for the MIF/3-FHC and MIF/4-FHC complexes is 1.01 and 0.95 Å, respectively, which is an indication that the generated NPT MD trajectories of these complexes were quite stable. For the other four complexes, the rmsd values and the total energy along the 1 ns NPT trajectory are very much similar to those of the MIF/4-FHC complex. During the simulation, no large conformational changes of MIF occur upon ligand binding, which is also in agreement with the heteronuclear ¹⁵N relaxation data of MIF that most of the backbone of MIF existed in a rigid structure of limited conformational flexibility on the nanosecond to picosecond time scale.³⁸

An obvious phenomenon was found from Figure 2 indicating that in the MIF/3-FHC complex the rmsd of C α is a little larger than that in the MIF/4-FHC complex. This implies that compared with MIF/4-FHC complex, MIF in the MIF/3-FHC complex undergoes slightly larger conformational changes after complex formation, which leads us to the hypothesis that the somewhat larger conformational changes of MIF in the MIF/3-FHC complex are obvious reflections of relatively weaker binding affinity of 3-FHC.

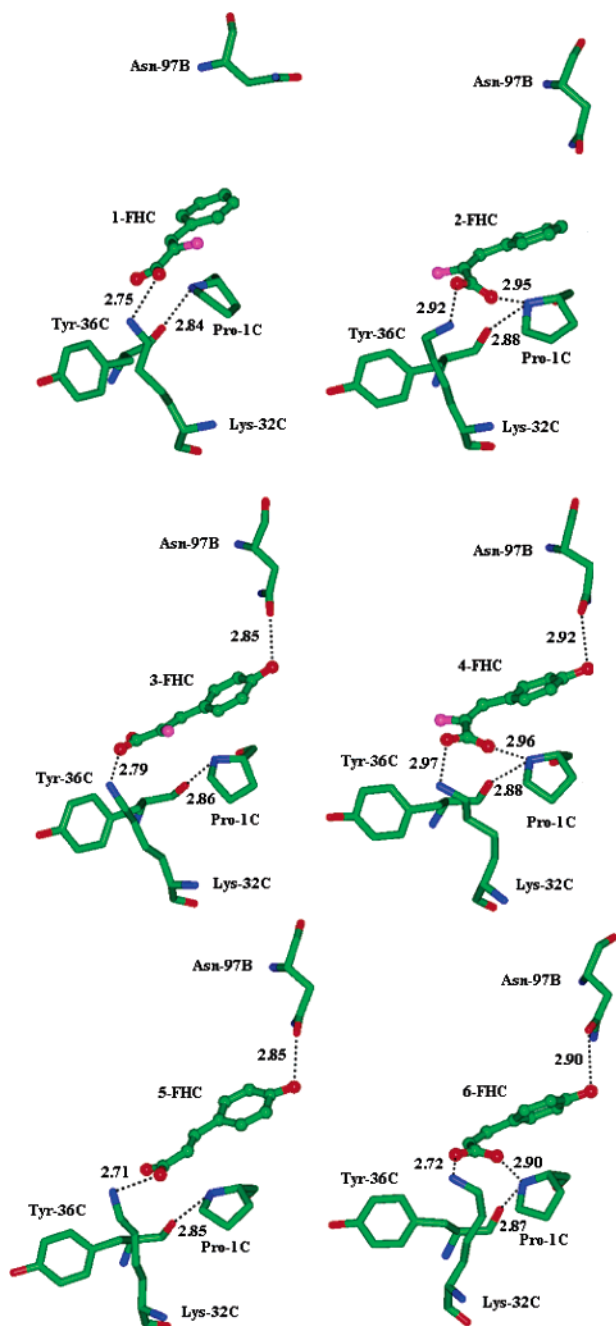


Figure 4. Hydrogen bonds and salt bridges between MIF and six ligands. Distances (Å) are measured from center to center of two heavy atoms. Symbols of the residues are explained in the text.

The active site of MIF, consisting of Pro-1, Met-2, Lys-32, Ile-64, Tyr-95' (where ' refers to the adjacent subunit), Asn-97', Val-106, and Phe-113, is located in a hydrophobic region that lies between two adjacent subunits of the homotrimer. Pro-1, Lys-32, and Ile-64, as the key residues involved in the catalytic reaction, are conserved residues among all MIF homologues (5-carboxymethyl-2-hydroxyruconate isomerase (CHMI), 4-oxalocrotonate tautomerase (4-OT), and chorismate mutase), whereas Tyr-95' and Asn-97' are not conserved.²⁵

The hydrogen bonds were examined on the basis of the trajectories of the MD simulations (Table 2). Figure 4 shows the hydrogen bonds between MIF and the six ligands.

Table 3. Calculated Energies and Dipole Moments of the Six Ligands

ligand	E_{tot} (gas) ^a	E_{tot} (water) ^a	SE ^b	μ ^c
1-FHC	-597.093 14 (0.00)	-597.184 69 (0.00)	57.45	13.26
2-FHC	-597.088 49 (2.92)	-597.175 46 (5.79)	54.57	9.95
3-FHC	-672.339 64 (0.00)	-672.442 09 (0.00)	64.29	15.56
4-FHC	-672.334 94 (2.95)	-672.432 84 (5.80)	61.43	12.60
5-FHC	-573.063 29 (0.00)	-573.172 32 (0.00)	68.42	17.02
6-FHC	-573.060 32 (1.86)	-573.162 84 (5.95)	72.13	12.85

^a Total energies are given in au. Listed in the parentheses are the relative energy (in kcal/mol) of the isomer with respect to the 1-FHC. ^b SE (in kcal/mol) is the energy difference between E_{tot} (gas) and E_{tot} (water). ^c In units of debye.

One hydrogen bond exists in MIF between the nitrogen of Pro-1C (where C refers to C subunit of MIF) and the carbonyl oxygen of Tyr-36C. Each *E*-ligand has an extra hydrogen bond between the carboxylate oxygen and the nitrogen of Pro-1C compared with the *Z*-ligand complex. Therefore, in complexes of MIF with all the *E*-ligands, Pro-1C has a bifurcated hydrogen bond. For the ligands that have the phenolic hydroxyl group, one more hydrogen bond was formed between the side chain carbonyl oxygen of Asn-97B (where B refers to the B subunit) and the phenolic hydroxyl group.

In addition, for all the ligands, a salt bridge is formed between one negative carboxylate oxygen and the positive NZ atom of the side chain of Lys-32C. The salt bridge may stabilize the binding of the ligands to MIF, which is especially true for 1-FHC because it has no hydrogen bond with MIF on complex formation. The averaged distances along the 1 ns NPT trajectory between the negative carboxylate oxygen atom of the ligands and the NZ atom of the side chain of Lys-32C are all below 3.0 Å.

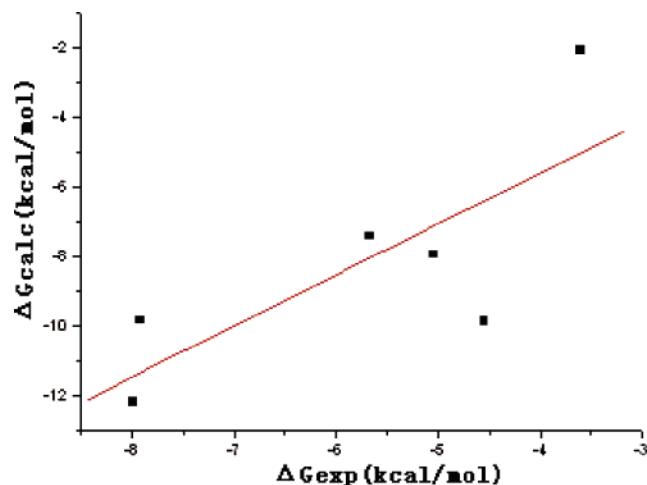
Comparison of the K_i of these *E*- and *Z*-ligands reveals a large difference in their binding affinities, which may be due to their different interactions with MIF. Though a salt bridge exists between ligands and MIF, it could not serve as an explanation to the large binding affinity difference in the same series of ligands. There is a hydrogen bond between Asn-97' and the phenolic hydroxyl group of the ligands. However, 1-FHC and 2-FHC have no phenolic hydroxyl group and their binding affinity difference could not be explained by hydrogen bond formation of Asn-97'. The distinct binding characteristic of *E*- and *Z*-ligands with Pro-1 may be the main cause of such a large difference in their binding affinities in the same series of ligand (1 and 2, 3, and 4, 5 and 6). This result is consistent with P1G and P1A MIF mutant studies,^{25,45} showing that Pro-1 is essential for the catalytic activity of MIF. The highly conserved N-terminal proline, surrounded by solvent-exposed residues, is located at the base of the hydrophobic pocket, which is highlighted by site-directed mutagenesis as a critical residue of the catalytic activity of MIF.^{25,45}

The intrinsic relative stability of these *Z*- and *E*-isomers was explored using quantum chemistry theory. The calculated results (Table 3) at the B3LYP/6-311++G-(d,p) level of theory show that all the *E*-ligands are higher in energy than the corresponding *Z*-ligands in the gas phase. This can be well ascribed to the steric effect between the carboxylate group and the aromatic ring in the *E*-ligands, and indeed, in these species, a nonplanar structure was observed, although there still exists C-H...O intramolecular hydrogen bonding be-

Table 4. Calculated Binding Free Energies (ΔG_{calc}) of Six Complexes vs Experimental Data (ΔG_{exp})^a

complex	ΔE_{ele}	ΔE_{vdw}	ΔE_{sur}	ΔE_{gas}	ΔE_{pbsol}	ΔE_{pbele}	ΔG_{calc} ^b	ΔG_{exp} ^c
MIF/1-FHC	-126.89	-23.75	-1.08	-150.64	148.57	22.76	-2.07	-3.611
MIF/2-FHC	-133.74	-24.36	-1.09	-158.09	150.67	18.03	-7.42	-5.674
MIF/3-FHC	-115.20	-25.72	-1.11	-140.92	131.04	16.95	-9.88	-4.552
MIF/4-FHC	-146.11	-26.56	-1.10	-172.67	162.84	17.83	-9.83	-7.914
MIF/5-FHC	-116.96	-26.04	-1.11	-143.00	135.05	19.21	-7.94	-5.044
MIF/6-FHC	-156.57	26.38	-1.15	-182.94	170.78	15.36	-12.17	-7.988

^a All energies are given in kcal/mol, and the symbols are explained in the text. ^b Calculation of ΔG_{calc} does not explicitly consider entropy contributions. ^c ΔG_{exp} is calculated from K_i (ref 8).

**Figure 5.** Calculated binding free energies (ΔG_{calc}) for the six analogues vs experimental data (ΔG_{exp}).

tween the oxygen atom of the carboxylate group and the hydrogen atom in the aromatic ring that may compensate the steric repulsion to some degree. When the solvent effect was considered in the calculations, the relative energy becomes larger for each *Z/E* pair, which is attributed to larger polarity of the *Z*-isomers (see dipole moment in Table 3). All these results indicate that *Z*-ligands are thermodynamically more stable than *E*-ligands, which is in accordance with the experiment.⁸ When located at the active sites of MIF, *Z*-ligands have weaker binding affinities than *E*-ligands, which may be explained by the more favorable interactions of *E*-ligands with MIF.

MM-PBSA using the single trajectory method had been performed to calculate binding free energies. The 51 snapshots were taken at even intervals from the last 400 ps of MD trajectories for analysis of the binding free energy. The calculated binding free energies are averaged from the 51 snapshots (Table 4). Considering the impracticality of normal mode calculations for the large size of these complexes and the uncertainties in the entropic calculation, entropic effects of the solute were not explicitly taken into account. For a series of compounds with similar structures and binding modes, the entropy contribution can be omitted if one is only interested in the relative order of binding affinities.¹⁷

A correlation coefficient of 0.77 between the calculated and experimental relative binding free energies was obtained (Figure 5), which shows that the energetic analysis performed by MM-PBSA is applicable to the current case study. The calculated relative binding free energy ($\Delta\Delta G_{\text{calc}}$) between the MIF/1-FHC and MIF/2-FHC complexes, 5.35 kcal/mol, is in agreement with the relative experimental energy ($\Delta\Delta G_{\text{exp}}$), 3.287 kcal/mol. For complexes MIF/5-FHC and MIF/6-FHC, the $\Delta\Delta G_{\text{calc}}$,

4.23 kcal/mol, is also in agreement with the corresponding $\Delta\Delta G_{\text{exp}}$, 2.944 kcal/mol. For complex MIF/3-FHC, its calculated free energy shows a large deviation from the experimental data and is smaller than that of complex MIF/4-FHC. This could be due to the somewhat overestimation of the relative stability of MIF/3-FHC.

The gas-phase electrostatic values, ΔE_{ele} of the six complexes, show that electrostatic interactions are in favor of the binding. However, the overall electrostatic interactions energies, ΔE_{pbele} , are positive and unfavorable for the binding, which is caused by the large desolvation penalty of charged and polar groups that is not sufficiently compensated upon complex formation. The ΔE_{ele} values of *Z*-ligands are much smaller than those of *E*-ligands, indicating that electrostatic interactions favor *E*-ligands more than corresponding *Z*-ligands, which is in agreement with the hydrogen bond analysis that each *E*-ligand has a hydrogen bond with Pro-1C and no hydrogen bonds were found between the *Z*-ligands and Pro-1C.

Although 1-FHC has no hydrogen bond with MIF, its ΔE_{ele} (-126.89 kcal/mol) contributes more to the binding than that of 3-FHC and 5-FHC (-115.20, -116.96 kcal/mol, respectively), which shows that the electrostatic interaction may come partly from the salt bridge formed with Lys-32C of MIF and the carboxylate group of 1-FHC.

The van der Waals interaction energies, ΔE_{vdw} of the six complexes contribute favorably to the binding. ΔE_{vdw} values for the complex of MIF with *E*-ligands are a little higher than those for the complex of MIF and *Z*-ligands because *E*-ligands fit more snugly within the active-site cavity and have a tighter binding to MIF than *Z*-ligands, adding nonpolar packing in the active site to a much deeper extent. The energy difference ΔE_{vdw} between these complexes is not large, which may indicate that van der Waals interactions are not an important factor for the binding affinity difference between *E*- and *Z*-ligands.

Conclusions

MD simulations together with MM-PBSA analysis were performed on six complexes to investigate the binding modes of six ligands and to evaluate their binding affinities. The large difference in their binding affinities is elucidated in detail with structural and energy analyses. The binding modes of *E*-ligands are much different from those of *Z*-ligands; i.e., *E*-ligands have hydrogen bonds with Pro-1C, while no hydrogen bond was found between *Z*-ligands and Pro-1C. This distinct binding characteristic of *E*- and *Z*-ligands with Pro-1 is in agreement with the previous report that Pro-1 is essential for the catalytic activity of MIF. MM-PBSA analysis successfully segregated different ener-

getic components. Electrostatic, van der Waals, and hydrophobic interactions are in favor of binding, whereas polar solvation is an unfavorable factor for the binding. Structural analysis and MM-PBSA analysis both show that the distinct binding characteristic of *E*- and *Z*-ligands with Pro-1 may be the main cause of the large difference in the binding affinities.

Acknowledgment. This work was supported by the P.H.D. Fund of Ningbo (Grant No. 2004A610010) and Ningbo Online Technology Market and Cooperation Project (Grant No. 2004A410049). We thank Prof. David A. Case from Scripps Research Institute for offering us the AMBER 7 package.

Supporting Information Available: The principal of calculation of binding free energies. This material is available free of charge via the Internet at <http://pubs.acs.org>.

References

- Calandra, T.; Roger, T. Macrophage migration inhibitory factor: a regulator of innate immunity. *Nat. Rev. Immunol.* **2003**, *3*, 791–800.
- Bernhagen, J.; Calandra, T.; Bucala, R. Regulation of the immune response by macrophage migration inhibitory factor: biological and structural features. *J. Mol. Med.* **1998**, *76*, 151–161.
- Sun, H. W.; Bernhagen, J.; Bucala, R.; Lolis, E. Crystal structure at 2.6 Å resolution of human macrophage migration inhibitory factor. *Proc. Natl. Acad. Sci. U.S.A.* **1996**, *93*, 5191–5196.
- Suzuki, M.; Sugimoto, H.; Nakagawa, A.; Tanaka, I.; Nishihara, J.; Sakai, M. Crystal structure of the macrophage migration inhibitory factor from rat liver. *Nat. Struct. Biol.* **1996**, *3*, 259–266.
- Donn, R. P.; Ray, D. W. Macrophage migration inhibitory factor: molecular, cellular and genetic aspects of a key neuroendocrine molecule. *J. Endocrinol.* **2004**, *182*, 1–9.
- Lolis, E. Glucocorticoid counter regulation: macrophage migration inhibitory factor as a target for drug discovery. *Curr. Opin. Pharmacol.* **2001**, *1*, 662–668.
- Rosengren, E.; Aman, P.; Thelin, S.; Hansson, C.; Ahlfors, S.; Bjork, P.; Jacobsson, L.; Rorsman, H. The macrophage migration inhibitory factor MIF is a phenylpyruvate tautomerase. *FEBS Lett.* **1997**, *417*, 85–88.
- Pirrung, M. C.; Chen, J.; Rowley, E. G.; Andrew, T. Mechanistic and stereochemical study of phenylpyruvate tautomerase. *J. Am. Chem. Soc.* **1993**, *115*, 7103–7110.
- Moth, C. W.; Prusakiewicz, J. J.; Marnett, L. J.; Lybrand, T. P. Stereoselective binding of indomethacin ethanamide derivatives to cyclooxygenase-1. *J. Med. Chem.* **2005**, *48*, 3613–3620.
- Krohn, A.; Redshaw, S.; Ritchie, J. C.; Graves, B. J.; Hatada, M. H. Novel binding mode of highly potent HIV-proteinase inhibitors incorporating the (*R*)-hydroxyethylamine isostere. *J. Med. Chem.* **1991**, *34*, 3340–3342.
- Holladay, M. W.; Salituro, F. G.; Rich, D. H. Synthetic and enzyme inhibition studies of pepstatin analogs containing hydroxyethylene and ketomethylene dipeptide isosteres. *J. Med. Chem.* **1987**, *30*, 374–383.
- Pereillo, J. M.; Maftouh, M.; Andrieu, A.; Uzabiaga, M. F.; Fedeli, O.; Savi, P.; Pascal, M.; Herbert, J. M.; Maffrand, J. P.; Picard, C. Structure and stereochemistry of the active metabolite of clopidogrel. *Drug Metab. Dispos.* **2002**, *30*, 1288–1295.
- Lam, P. Y. S.; Ru, Y.; Jadhav, P. K.; Aldrich, P. E.; DeLuca, G. V.; Eyermann, C. J.; Chang, C.-H.; Emmett, G.; Holler, E. R.; Daneker, W. F.; Li, L.; Confalone, P. N.; McHugh, R. J.; Han, Q.; Li, R.; Markwalder, J. A.; Seitz, S. P.; Sharpe, T. R.; Bachelier, L. T.; Rayner, M. M.; Klabe, R. M.; Shum, L.; Winslow, D. L.; Kornhauser, D. M.; Jackson, D. A.; Erickson-Viitanen, S.; Hodge, C. N. Cyclic HIV protease inhibitors: synthesis, conformational analysis, P2/P2' structure–activity relationship, and molecular recognition of cyclic ureas. *J. Med. Chem.* **1996**, *39*, 3514–3525.
- Kollman, P. A.; Massova, I.; Reyes, C.; Kuhn, B.; Huo, S.; Chong, L.; Lee, M.; Lee, T.; Duan, Y.; Wang, W.; Donini, O.; Cieplak, P.; Srinivasan, J.; Case, D. A.; Cheatham, T. E., III Calculating structures and free energies of complex molecules: combining molecular mechanics and continuum models. *Acc. Chem. Res.* **2000**, *33*, 889–897.
- Huo, S.; Wang, J.; Cieplak, P.; Kollman, P. A.; Kuntz, I. D. Molecular dynamics and free energy analyses of cathepsin D–inhibitor interactions: insight into structure-based ligand design. *J. Med. Chem.* **2002**, *45*, 1412–1419.
- Bonnet, P.; Richard, A.; Bryce, R. A. Molecular dynamics and free energy analysis of neuraminidase–ligand interactions. *Protein Sci.* **2004**, *13*, 946–957.
- Wang, J. M.; Morin, P.; Wang, W.; Kollman, P. A. Use of MM-PBSA in reproducing the binding free energies to HIV-1 RT of TIBO derivatives and predicting the binding mode to HIV-1 RT of efavirenz by docking and MM-PBSA. *J. Am. Chem. Soc.* **2001**, *123*, 5221–5230.
- Kuhn, B.; Kollman, P. A. Binding of a diverse set of ligands to avidin and streptavidin: an accurate quantitative prediction of their relative affinities by a combination of molecular mechanics and continuum solvent models. *J. Med. Chem.* **2000**, *43*, 3786–3791.
- Spackova, N.; Cheatham, T. E., III; Ryjacek, F.; Lankas, F.; van Meervelt, L.; Hobza, P.; Sponer, J. Molecular dynamics simulations and thermodynamics analysis of DNA–drug complexes. Minor groove binding between 4',6-diamidino-2-phenylindole and DNA duplexes in solution. *J. Am. Chem. Soc.* **2003**, *125*, 1759–1769.
- Reyes, C. M.; Kollman, P. A. Structure and thermodynamics of RNA–protein binding: using molecular dynamics and free energy analyses to calculate the free energies of binding and conformational change. *J. Mol. Biol.* **2000**, *297*, 1145–1158.
- Lee, M. R.; Duan, Y.; Kollman, P. A. Use of MM-PB/SA in estimating the free energies of proteins: Application to native, intermediates, and unfolded villin headpiece. *Proteins* **2000**, *39*, 309–316.
- Taylor, A. B.; Johnson, W. H., Jr.; Czerwinski, R. M.; Li, H. S.; Hackert, M. L.; Whitman, C. P. Crystal structure of macrophage migration inhibitory factor complexed with (*E*)-2-fluoro-*p*-hydroxycinnamate at 1.8 Å resolution: implications for enzymatic catalysis and inhibition. *Biochemistry* **1999**, *38*, 7444–7452.
- DS Modeling*, release 1.1; Accelrys Inc.: San Diego, CA, 2003.
- Rizzo, R. C.; Toba, S.; Kuntz, I. D. A molecular basis for the selectivity of thiazazole urea inhibitors with stromelysin-1 and gelatinase-a from generalized Born molecular dynamics simulations. *J. Med. Chem.* **2004**, *47*, 3065–3074.
- Lubetsky, J. B.; Swope, M.; Dealwis, C.; Blake, P.; Lolis, E. Pro-1 of macrophage migration inhibitory factor functions as a catalytic base in the phenylpyruvate tautomerase activity. *Biochemistry* **1999**, *38*, 7346–7354.
- Case, D. A.; Pearlman, D. A.; Caldwell, J. W.; Cheatham, T. E., III; Wang, J.; Ross, W. S.; Simmerling, C. L.; Darden, T. A.; Merz, K. M.; Stanton, R. V.; Cheng, A. L.; Vincent, J. J.; Crowley, M.; Tsui, V.; Gohlke, H.; Radmer, R. J.; Duan, Y.; Pitera, J.; Massova, I.; Seibel, G. L.; Singh, U. C.; Weiner, P. K.; Kollman, P. A. *AMBER 7*; University of California: San Francisco, 2002.
- Jorgensen, W. L.; Chandrasekhar, J.; Madura, J. D.; Impey, R. W.; Klein, M. L. Comparison of simple potential functions for simulating liquid water. *J. Chem. Phys.* **1983**, *79*, 926–935.
- Cornell, W. D.; Cieplak, P.; Bayly, C. I.; Gould, I. R.; Merz, K. M., Jr.; Ferguson, D. M.; Spellmeyer, D. C.; Fox, T.; Caldwell, J. W.; Kollman, P. A. *J. Am. Chem. Soc.* **1995**, *117*, 5179–5197.
- Frisch, M. J.; Trucks, G. W.; Schlegel, H. B.; Scuseria, G. E.; Robb, M. A.; Cheeseman, J. R.; Zakrzewski, V. G.; Montgomery, J. A., Jr.; Stratmann, R. E.; Burant, J. C.; Dapprich, S.; Millam, J. M.; Daniels, A. D.; Kudin, K. N.; Strain, M. C.; Farkas, O.; Tomasi, J.; Barone, V.; Cossi, M.; Cammi, R.; Mennucci, B.; Pomelli, C.; Adamo, C.; Clifford, S.; Ochterski, J.; Petersson, G. A.; Ayala, P. Y.; Cui, Q.; Morokuma, K.; Malick, D. K.; Rabuck, A. D.; Raghavachari, K.; Foresman, J. B.; Cioslowski, J.; Ortiz, J. V.; Stefanov, B. B.; Liu, G.; Liashenko, A.; Piskorz, P.; Komaromi, I.; Gomperts, R.; Martin, R. L.; Fox, D. J.; Keith, T.; Al-Laham, M. A.; Peng, C. Y.; Nanayakkara, A.; Gonzalez, C.; Challacombe, M.; Gill, P. M. W.; Johnson, B. G.; Chen, W.; Wong, M. W.; Andres, J. L.; Head-Gordon, M.; Replogle, E. S.; Pople, J. A. *Gaussian 98*, revision A7; Gaussian, Inc.: Pittsburgh, PA, 1998.
- Besler, B. H.; Merz, K. M.; Kollman, P. A. Atomic charges derived from semiempirical methods. *J. Comput. Chem.* **1990**, *11*, 431–439.
- Fox, T.; Kollman, P. A. Application of the RESP methodology in the parametrization of organic solvents. *J. Phys. Chem. B* **1998**, *102*, 8070–8079.
- Becke, A. D. Density-functional thermochemistry. III. The role of exact exchange. *J. Chem. Phys.* **1993**, *98*, 5648–5652.
- Lee, C.; Yang, W. T.; Parr, R. G. Development of the Colle–Salvetti correlation-energy formula into a functional of the electron density. *Phys. Rev. B* **1988**, *37*, 785–789.
- Hehre, W.; Radom, L.; Schleyer, P. V. R.; Pople, J. A. *Ab Initio Molecular Orbital Theory*; Wiley: New York, 1986.
- Miertus, S.; Scrocco, E.; Tomasi, J. Electrostatic interaction of a solute with a continuum. A direct utilization of ab initio molecular potentials for the prevision of solvent effects. *Chem. Phys.* **1981**, *55*, 117–129.
- Darden, T.; York, D.; Pedersen, L. Particle mesh Ewald: An $N \log(N)$ method for Ewald sums in large systems. *J. Chem. Phys.* **1993**, *98*, 10089–10092.

- (37) Ryckaert, J. P.; Ciccotti, G.; Berendsen, H. J. C. Numerical integration of the Cartesian equations of motion of a system with constraints: molecular dynamics of *n*-alkanes. *J. Comput. Phys.* **1977**, *23*, 327–341.
- (38) Muhlhahn, P.; Bernhagen, J.; Czisch, M.; Georgescu, J.; Renner, C.; Ross, A.; Bucalaand, R.; Holak, T. A. NMR characterization of structure, backbone dynamics, and glutathione binding of the human macrophage migration inhibitory factor. *Protein Sci.* **1996**, *5*, 2095–2103.
- (39) Massova, I.; Kollman, P. A. Combined molecular mechanical and continuum solvent approach (MM-PBSA/GBSA) to predict ligand binding. *Perspect. Drug Discovery Des.* **2000**, *18*, 113–135.
- (40) Honig, B.; Nicholls, A. Classical electrostatics in biology and chemistry. *Science* **1995**, *268*, 1144–1149.
- (41) Sitkoff, D.; Sharp, K. A.; Honig, B. Accurate calculation of hydration free energies using macroscopic solvent models. *J. Phys. Chem.* **1994**, *98*, 1978–1988.
- (42) Connolly, M. L. Analytical molecular surface calculation. *J. Appl. Crystallogr.* **1983**, *16*, 548–558.
- (43) Srinivasan, J.; Cheatham, T. E., III; Cieplak, P.; Kollman, P. A.; Case, D. A. Continuum solvent studies of the stability of DNA, RNA, and phosphoramidate–DNA helices. *J. Am. Chem. Soc.* **1998**, *120*, 9401–9409.
- (44) Gohlke, H.; Case, D. A. Converging free energy estimates: MM-PB(GB)SA studies on the protein–protein complex ras–raf. *J. Comput. Chem.* **2004**, *25*, 238–250.
- (45) Stamps, S. L.; Taylor, A. B.; Wang, S. C.; Hackert, M. L.; Whitman, C. P. Mechanism of the phenylpyruvate tautomerase activity of macrophage migration inhibitory factor: properties of the P1G, P1A, Y95F, and N97A mutants. *Biochemistry* **2000**, *39*, 9671–9678.

JM050562Z